NANOSTRUCTURED BORON-DOPED DIAMOND ELECTRODES FOR ENHANCED HEAVY METAL SENSING

G M Hasan Ul Banna[1,2], James R Siegenthaler[1,3], Ahmed Azwad Kabir[1], Raul Murillo Martinez[4], and Wen Li[1,2,3]*

[1]Department of Electrical and Computer Engineering, Michigan State University, East Lansing, MI, USA

[2]Institute for Quantitative Health Science & Engineering, Michigan State University, East Lansing, MI, USA

[3]Fraunhofer USA Center Midwest, East Lansing, MI, USA

[4]Department of Mechanical Engineering, Michigan State University, East Lansing, MI, USA

2025 IEEE 38th International Conference on Micro Electro Mechanical Systems (MEMS) | 979-8-3315-0889-0/25/$31.00 ©2025 IEEE | DOI: 10.1109/MEMS61431.2025.10917425

ABSTRACT

This paper presents a novel fabrication technique that enables the precise formation of nanostructures on targeted regions of boron-doped diamond (BDD) electrodes. The process utilizes a custom-grown porous anodic aluminum oxide (AAO) template created by anodization, followed by reactive ion etching (RIE) to transfer the nanostructures from the AAO template to the BDD surface. This method eliminates the need for complex two-step diamond synthesis approaches and is more time- and cost-efficient. The fabricated nanostructured BDD (NSBDD) surface increases the electrochemical active surface area by 556% with nanostructures on the surface that helps to lower the limit of detection (LOD) significantly in heavy metal sensing.

KEYWORDS

Anodic aluminum oxide, Boron-doped diamond, Heavy metal sensing, Nanostructured electrode

INTRODUCTION

Over the past few decades, there has been a growing fascination with boron-doped diamond (BDD) electrodes, primarily because of their distinctive characteristics. These properties encompass an exceptionally wide electrochemical potential range, a minimal and consistent background current, low capacitance, remarkable resistance to biofouling, and a high degree of biocompatibility [1]. Typically, BDD shows a potential window from -1.5 V to +3 V vs standard hydrogen reference electrode in aqueous 1 M H_2SO_4 [2]. This wide potential window allows for the detection of multiple heavy metals that have different reduction or oxidation potentials in this wide range [3]. Moreover, it helps to reduce the overlapping of peaks between heavy metals and allows clearer, more distinct detection of individual heavy metals. Despite these benefits, pristine BDD electrodes are always overlooked for their lower sensitivity compared to other carbon-based materials due to the BDD's resistance to surface adsorption. BDD has found diverse applications spanning energy storage, electrocatalysis, biosensors, environmental monitoring, water treatment, and more [4]. For the improvement of sensing performance, a number of ways have been explored, including the increment of sensing probe numbers, introducing microelectrode arrays, embedding nanomaterials, electrochemical pretreatment, surface functionalization using nanocomposite and polymers [4], [5], [6].

In this study, we have modified the BDD electrode fabrication process with custom-grown porous anodic aluminum oxide (AAO) by anodization, followed by reactive ion etching (RIE) to achieve a nanostructured BDD (NSBDD) electrode surface. This NSBDD surface increases the electrochemical active surface area by introducing nanostructures on the surface that help to drive heavy metal sensing performance. Here, we characterized the surface with scanning electron microscopy (SEM), atomic force microscopy (AFM), and Raman spectroscopy, investigating surface changes induced by RIE. We then analyzed the roughened surface responses electrochemically and verified the increase in the electroactive area through cyclic voltammetry (CV). We then investigated the utility of these NSBDD electrodes for in situ measurement of heavy metal ions in acetate buffer, including Cd^{2+}, Pb^{2+}, and Hg^{2+}.

FABRICATION PROCESS

The electrically conductive BDD layer was grown on a nonconductive 1 mm thick 4-inch diameter (100) Si wafer using a dedicated in-house built 915 MHz microwave plasma-assisted chemical vapor deposition (MWCVD) reactor. The growth was done using the following parameters: 60 Torr pressure, 9 kW absorbed microwave power, the stage temperature of 900 ºC, and a gas chemistry of 2% methane in hydrogen, to ensure the diamond quality. Diborane was introduced during the deposition to ensure conductivity with B/C ratio of 37,500 ppm. Then, a 500 nm aluminum (Al) layer was deposited using a thermal evaporator (Edward Auto306 thermal evaporator, Edwards, Inc.). Then the Al coated 4-inch wafer was mechanically cleaved into small pieces (1×1 inch), and cleaned ultrasonically in acetone, isopropanol, and deionized water for 10 minutes each before anodization. The Al thin film coated BDD pieces were used as an anode and a 70 mm length and 3 mm diameter graphite rod was used as a cathode. A 0.5 v% phosphoric acid was used as the solvent. Anodization was performed in potentiostatic mode with an input voltage of 5 V at room temperature. DC voltage was controlled by a power supply (Agilent Keysight 6634A System DC Power Supply, Hewlett Packard, Palo Alto, CA, USA). The AAO process was run for 15 min with continuous stirring.

The anodized samples were used directly as a templated mask for RIE. A reactive ion plasma dry etcher (RIE-ICP, Trion technology, Tempe, Az, USA) was used

to etch the anodized templated BDD with a gas mixture of 3 SCCM of SF_6, 10 SCCM of Argon, and 30 SCCM of O_2 at 10 mTorr pressure and 500 W ICP, and 150 W RIE power resulting a DC bias voltage of 90 V. This process was run for 15 min, 25 min, and 35 min to prepare three sets of test samples. Finally, the samples were cleaned with concentrated hydrochloric acid at 200 ºC for 2 min to remove residual Al. These samples were further cleaned in 1 M H_2SO_4 solution before each measurement with a 3 V constant potential for 120 s and a -3 V constant potential for another 120 s to active NSBDD surface. Figure 1 shows the schematic process for the NSBDD fabrication.

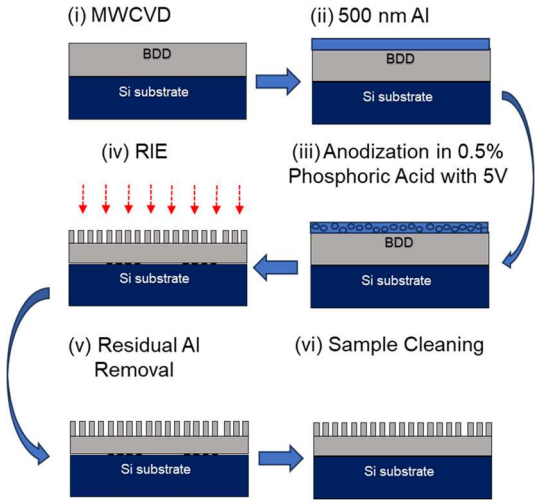

Figure 1 Schematic process for NSBDD fabrication

SURFACE ANALYSIS

SEM images of the NSBDD samples are shown in Figure 2 (i) and (ii) are for untreated BDD samples representing the topology at 5° tilted angle and cross section at 27° tilted angle, respectively. Then Figure 2 (iii) shows the top view photograph after anodization of Al layer on BDD samples. The inset image clearly shows the mesh like porous structure on the BDD samples, which were achieved by the anodization process as described earlier. Then Figure 2 (iv), (v), and (vi) shows the 15 min, 25 min, and 35 min RIE treated BDD samples, respectively. These topographic images, taken at a 5° tilt, clearly show the nanostructures on the BDD samples. With increasing RIE time the number of nanostructures has increased in the same sampling area.

The developed nanostructures on BDD were characterized using AFM and Raman spectroscopy. Figure 3 shows the AFM topographic response of the BDD surface changes due to RIE. As expected, the roughness increased from the as received to 15 min RIE by 44.2 nm, 25 min RIE by 299 nm, and 35 min RIE sample by 699 nm. This AFM analysis also confirms the roughness change with RIE on NSBDD surface. Figure 4 quantifies the roughness measurement with respect to RIE time.

Raman spectroscopy, a nondestructive tool, was used for analysis of each sample. The goal is to identify if the carbon content changed (ratio of sp^2 to sp^3) due to long and harsh RIE treatment. Figure 5 shows the Raman spectra of as-received (bare) BDD and different time RIE-treated NSBDD. In all the spectra, a broad scattering intensity at 480 cm^{-1} is observed, this has been attributed to the vibrational modes of boron dimers, pairs, and clusters [7]. The peak at 1200 cm^{-1} is assigned to the defects in diamond lattice and the 1332 cm^{-1} is assigned to the first order diamond phonon line which represents the boron doping concentration in BDD [8]. Finally, the peak at 1545 cm^{-1} represents the sp^2 carbon impurity that occurs at the grain boundary of the high boron doping level [9]. No noticeable changes were observed in sp^2 and sp^3 peaks in all the Raman spectra from bare to RIE treated NSBDD sample. Moreover, we analyzed the peak intensity ratio among two peaks at 1332 cm^{-1} and 1545 cm^{-1} and found the ratio is 1.42 in all spectrums. This analysis confirms that there is no change of carbon allotrope after RIE treatments. Therefore, the diamond quality was preserved even with long and harsh RIE treatments.

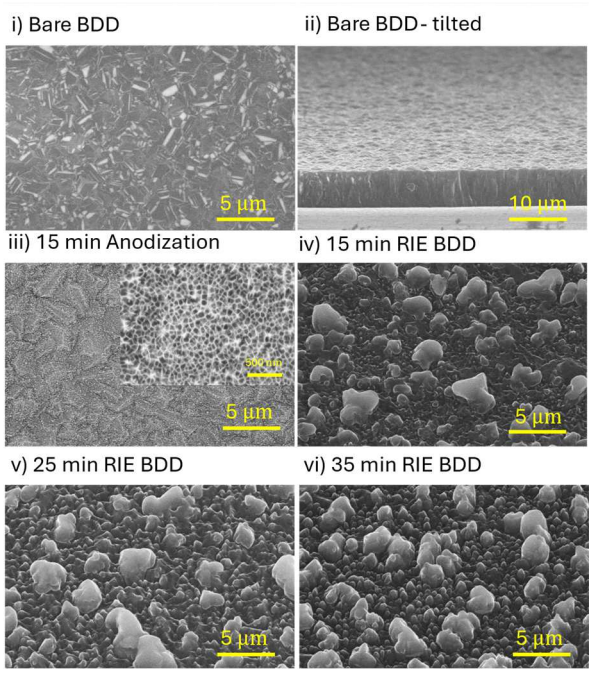

Figure 2 SEM images show (i) a top view, (ii) a tilted cross-sectional view of bare BDD. Top view of (iii) Al anodization and RIE treated BDD for (iv) 15 min, (v) 25 min, (vi) 35 min.

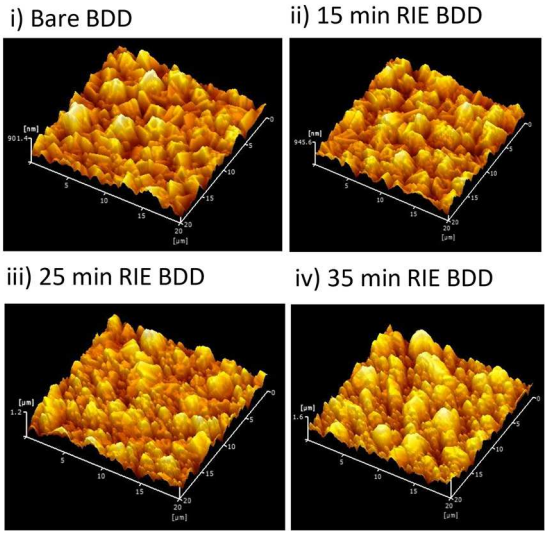

Figure 3 AFM images of NSBDD: (a) as received (z= 901.4 nm); and after RIE for: (b) 15 min (z= 945.6 nm), (c) 25 min (z= 1.2 µm), and (d) 35 min (z= 1.6 µm)

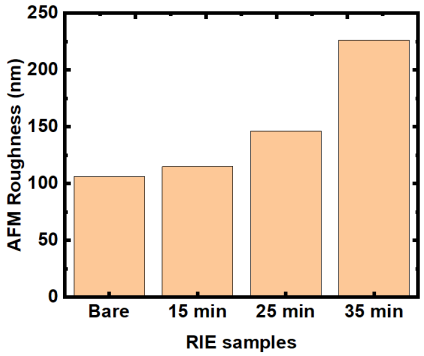

Figure 4 AFM roughness calculation in NSBDD

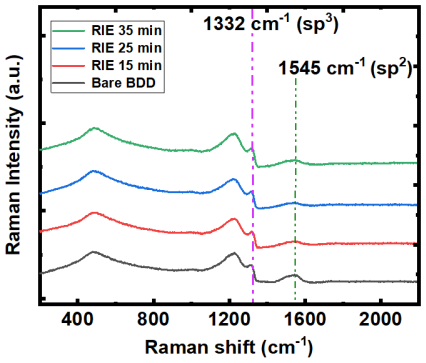

Figure 5 Raman spectra of NSBDD samples using different times of RIE. For comparison, as-received (untreated) BDD sample is also included.

MEASUREMENT SETUP

All the electrochemical measurements were taken using a CH Instruments (CHI6149E) potentiostat (CH Instruments, Inc. Austin, USA) in a three-electrode mode. The NSBDD was used as a working electrode (WE), an Ag/AgCl electrode (purchased from CH Instruments, Inc. Austin, USA) as a reference electrode (RE), and a Pt wire as a counter electrode (CE). Differential pulse stripping voltammetry (DP-ASV) was performed to validate the heavy metal sensing performance of the BDDs as follows: a plating deposition of -1.1 V for 120 s, followed by a voltage stripping ramp up to 0.6 V with a frequency of 60 Hz, an amplitude of 40 mV, and an increment voltage of 2 mV. These values are effectively chosen so that the targeted heavy metals can be resolved, and BDD surfaces are not over oxidized. All electrochemical experiments were run at room temperature inside a Faraday cage to minimize external electrical noises and all potentials reported are against the Ag/AgCl RE. A glass cell was mechanically attached to the BDD surface. To ensure the electrical connection, a copper plate was attached to the Si side of the samples and the WE connection was made so that the BDD surface and Cu plate were both connected.

ELECTROCHEMICAL ANALYSIS

Electrochemical characterization of the prepared NSBDD samples was done by performing CVs on 2 mM $[Fe(CN)_6]^{3-/4-}$. The electron transfer kinetics toward the $[Fe(CN)_6]^{3-/4-}$ couple (inner sphere electron transfer) is sensitive to the BDD surface morphology. CVs of $[Fe(CN)_6]^{3-/4-}$ are presented in inset of Figure 6 with a scan rate of 0.10 V s^{-1}.

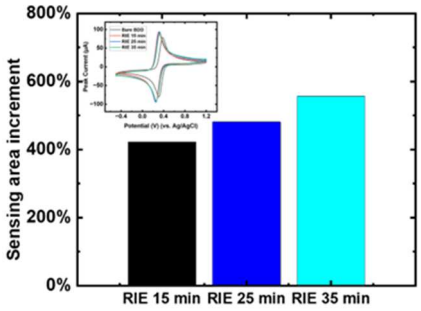

Figure 6 Percentage increment in the electrochemical effective sensing area measurement. Inset is the Cyclic voltammograms of the redox systems $[Fe(CN)_6]^{3-/4-}$ in 1 mol L^{-1} KCl recorded on bare and NSBDD films with a scan rate of 0.10 V s^{-1}.

Later, the effective sensing area of the NSBDD was measured using CV in a 2 mM $[Fe(CN)_6]^{3-/4-}$ solution containing 1 M KCl with 0.01 V s^{-1} scan rates based on the steady-state current equation [10], [11].

$$i_{ss} = 4nFDCr$$

where i_{ss} (A) is the steady-state current, n is the number of transported electrons, F is the Faradays constant, D ($cm^2 \cdot s^{-1}$) is the diffusion coefficient of the used redox marker (7.6×10^{-6} cm^2 s^{-1}), C ($mol \cdot cm^{-3}$) is the concentration of redox species, and r (cm) is the electrode radius. Figure 6 shows the increment of electrochemical sensing area increment in the RIE treated samples. It has been noticed that with increasing RIE treatment time, the effective surface area (A_{eff}) in NSBDD also increases. This is attributed to the increasing number of nanostructures in the NSBDD sample.

HEAVY METAL DETECTION USING NANOSTRUCTURED BDD SAMPLES

Finally, the untreated BDD and NSBDD were used to detect Cd^{2+}, Pb^{2+}, or Hg^{2+} in mixtures of the metals in 0.01 M acetate buffer (pH = 4.97) containing 50 mM NaCl solution with 10-1600 µg/L of each metal. Figure 7 shows three peaks at around -0.77 V, -0.55 V, and +0.1 V were detected for Cd^{2+}, Pb^{2+}, and Hg^{2+}, respectively, in one single DP-ASV measurement for (i) untreated BDD, (ii) 15 min RIE treated BDD, (iii) 25 min RIE treated BDD, and (iii) 35 min RIE treated BDD, respectively. This represents good selectivity over the range of heavy metal concentrations. These experiments were repeated on n=3 samples. The amplitude of the current peak is linearly related to the concentration, as demonstrated in Figure 7. The calculated limit of detection (LOD) for the three metals of untreated and treated BDD are summarized in Table 1.

Table 1. LOD comparison using NSBDD for Cd^{2+}, Pb^{2+}, and Hg^{2+} detection.

Sample	Cd^{2+}, PPB	Pb^{2+}, PPB	Hg^{2+}, PPB
Bare BDD	21.14	16.30	12.89
RIE 15 min	18.44	16.62	11.65
RIE 25 min	18.18	14.29	11.56
RIE 35 min	17.34	9.79	10.08

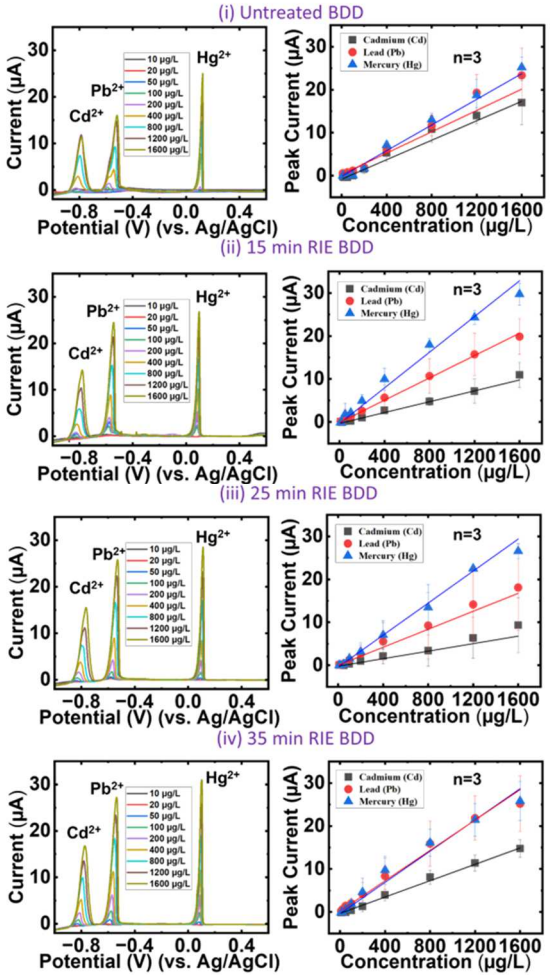

Figure 7 Heavy metal detection using NSBDD samples. Detection of 10, 20, 50, 100, 200, 400, 800, 1200, and 1600 μg/L concentrations of Cd^{2+}, Pb^{2+}, and Hg^{2+} mixture in buffer solution (pH=4.9) using i) untreated BDD, ii) 15 min RIE BDD, iii) 25 min RIE BDD, and iv) 35 min RIE BDD as WE

CONCLUSION

We successfully presented a custom process to develop NSBDD films. Morphological investigation through SEM and AFM shows the increasing number of nanostructures by treating the film longer with RIE. We also showed electrochemical characteristics by CV measurements and confirmed the A_{eff} increment with RIE-treated films. Moreover, the sp^2 and sp^3 content in the treated films did not change, and their ratio was the same throughout the samples. Finally, we showed successful detection of Cd^{2+}, Pb^{2+}, and inorganic Hg^{2+} metals in buffer solutions using NSBDD WE. RIE-treated samples showed improved LOD for all the metals due to the increase in the effective electrochemical area. These new NSBDD sensors will enable increased sensitivity in applications not only in environmental heavy metal sensing but also in electrocatalysis, biosensing, water treatment, and more.

ACKNOWLEDGEMENTS

This work was supported by the National Science Foundation (Award Number: 2226500). The authors appreciate Dr. Nina Baule's help with AFM measurements.

REFERENCES

[1] K. Muzyka, J. Sun, T. Haile Fereja, Y. Lan, W. Zhang, and G. Xu, "Boron-doped diamond: current progress and challenges in view of electroanalytical applications," *Analytical Methods*, vol. 11, no. 4, pp. 397–414, 2019, doi: 10.1039/C8AY02197J.

[2] E. A. McGaw and G. M. Swain, "A comparison of boron-doped diamond thin-film and Hg-coated glassy carbon electrodes for anodic stripping voltammetric determination of heavy metal ions in aqueous media," *Analytica Chimica Acta*, vol. 575, no. 2, pp. 180–189, Aug. 2006, doi: 10.1016/j.aca.2006.05.094.

[3] S. Kim *et al.*, "Development of boron doped diamond electrodes material for heavy metal ion sensor with high sensitivity and durability," *Journal of Materials Research and Technology*, vol. 23, pp. 1375–1385, Mar. 2023, doi: 10.1016/j.jmrt.2023.01.116.

[4] Y. Einaga, "Boron-Doped Diamond Electrodes: Fundamentals for Electrochemical Applications," *Acc. Chem. Res.*, vol. 55, no. 24, pp. 3605–3615, Dec. 2022, doi: 10.1021/acs.accounts.2c00597.

[5] C. A. Rusinek *et al.*, "All-Diamond Microfiber Electrodes for Neurochemical Analysis," *J. Electrochem. Soc.*, vol. 165, no. 12, p. G3087, Jul. 2018, doi: 10.1149/2.0141812jes.

[6] E. K. Purcell *et al.*, "Next-Generation Diamond Electrodes for Neurochemical Sensing: Challenges and Opportunities," *Micromachines*, vol. 12, no. 2, Art. no. 2, Feb. 2021, doi: 10.3390/mi12020128.

[7] V. A. Sidorov and E. A. Ekimov, "Superconductivity in diamond," *Diamond and Related Materials*, vol. 19, no. 5, pp. 351–357, May 2010, doi: 10.1016/j.diamond.2009.12.002.

[8] P. W. May, W. J. Ludlow, M. Hannaway, P. J. Heard, J. A. Smith, and K. N. Rosser, "Raman and conductivity studies of boron-doped microcrystalline diamond, facetted nanocrystalline diamond and cauliflower diamond films," *Diamond and Related Materials*, vol. 17, no. 2, pp. 105–117, Feb. 2008, doi: 10.1016/j.diamond.2007.11.005.

[9] R. F. Brocenschi, K. Irikura, N. Wachter, G. M. Swain, and R. C. Rocha-Filho, "Electrochemical surface rehydrogenation of boron-doped diamond electrodes after electrochemical polishing," *Diamond and Related Materials*, vol. 136, p. 110008, Jun. 2023, doi: 10.1016/j.diamond.2023.110008.

[10] R. Trouillon, Y. Lin, L. J. Mellander, J. D. Keighron, and A. G. Ewing, "Evaluating the Diffusion Coefficient of Dopamine at the Cell Surface During Amperometric Detection: Disk vs Ring Microelectrodes," *Anal. Chem.*, vol. 85, no. 13, pp. 6421–6428, Jul. 2013, doi: 10.1021/ac400965d.

[11] A. J. Bard and L. R. Faulkner, "Electrochemical methods: fundamentals and applications," *Surf. Technol*, vol. 20, no. 1, pp. 91–92, 1983.

CONTACT

*G M Hasan Ul Banna, tel: +1-517-6194884; bannag@msu.edu